Dynamics and function of ERM proteins during cytokinesis in human cells

Shota Hiruma[1], Tomoko Kamasaki[2], Kohei Otomo[3], Tomomi Nemoto[3], and Ryota Uehara[1, 4]

[1]Graduate School of Life Science, Hokkaido University, Japan

[2]Institute for Genetic Medicine, Hokkaido University, Japan

[3]Research Institute for Electronic Science, Hokkaido University, Japan

[4] Creative Research Institution, Hokkaido University, Japan

Correspondence
Ryota Uehara, Creative Research Institution, Hokkaido University, Kita-ku, Sapporo 001-0021, Japan
Fax: 81-11-706-9238
Tel: 81-11-706-9238
E-mail: ruehara@sci.hokudai.ac.jp

Running title: ERMs in cytokinesis

Keywords: Cytokinesis; Ezrin/Radixin/Moesin
Abbreviations: ERMs, Ezrin/Radixin/Moesin proteins; PIP2, phosphatidylinositol 4,5-bisphosphate; MbCD, methyl-b-cyclodextrin

Summary

The molecular mechanism that governs cytoskeleton—membrane interaction during animal cytokinesis remains elusive. Here, we investigated the dynamics and functions of ERM (Ezrin/Radixin/Moesin) proteins during cytokinesis in human cultured cells. We found that ezrin is recruited to the cleavage furrow through its membrane-associated domain in a cholesterol-dependent but largely Rho-independent manner. While ERMs are dispensable for furrow ingression, they play a pivotal role in contractile activity of the polar cortex. Notably, when anillin and supervillin are co-depleted, ERMs increasingly accumulate at the cleavage furrow and substantially contribute to the furrow ingression. These results reveal a supportive role of ERMs in cortical activities during cytokinesis, and alsoprovide insight into the selective mechanism that preferentially associates cytokinesis-relevant proteins with the division site.

Introduction

During cytokinesis in animal cells, there is drastic remodeling of actin-membrane interactions, which control global cell shape changes to separate a cell into two daughters. At the cell equator, an actin-based structure called the contractile ring transiently forms and drives the ingression of the equatorial membrane, while the cell cortex at the polar region gets relaxed to allow for cell elongation or to keep global force balance during cell deformation [1-5]. However, the molecular mechanisms that govern the dynamic reorganization of the cytoskeleton-membrane interface remain largely unknown. Interactions between the actin cytoskeleton and the plasma membrane in dynamic cellular processes are generally mediated by F-actin-binding and membrane-associated proteins [6,7]. Among numerous proteins in that category, anillin plays a pivotal role in cytokinesis control. Anillin directly binds to actin and myosin through its N-terminal domains and to RhoA or phosphatidylinositol 4,5-bisphosphate (PIP2) through its C-terminal domains, and it localizes to the cell equator throughout cytokinesis [8-13]. In the absence of anillin, the initial ingression of the cleavage furrow still takes place. However, in the course of furrow ingression, the contractile ring becomes delocalized from the cell equator, often resulting in ectopic oscillatory contraction of the polar cortex and eventual furrow regression [10,11]. Therefore, whereas precise and persistent control of membrane invagination is lost in the absence of anillin, gross cell shape change still occurs possibly through functions of other F-actin- and membrane-associated proteins during cytokinesis.

Besides anillin, an F-actin-binding and membrane-associated protein supervillin has been reported to play an important role in cytokinesis control. Supervillin possesses both actin and myosin binding domains within its N-terminal domain, through which it localizes to the cleavage furrow in mammalian cells [14,15]. Supervillin tightly binds to the isolated plasma membrane [16,17], though the protein domain corresponding to this binding has not been identified. Depletion of supervillin causes reduction in the active form of myosin II at the cleavage furrow and increases frequency of cytokinesis failure, indicating its active involvement in cytokinesis control [14,18,19].

Other well-conserved F-actin-binding and membrane-associated proteins that localize at the cleavage furrow are Ezrin/Radixin/Moesin proteins (ERMs). ERMs possess N-terminal FERM domain that associates with several membrane-associated proteins and C-terminal F-actin binding domain, and, therefore, function as linkers between actin cytoskeleton and the plasma membrane [20-22]. Previous studies have clarified the important roles of ERMs in various cellular processes such as epithelial morphogenesis, cell migration, and cell signal transduction [23-25]. Function of ERMs is regulated through their binding to PIP2 and subsequent phosphorylation, which relieves the proteins from their inactive form and enables their interaction with F-actin and the membrane [26-30]. Because ERMs prominently accumulate at the cleavage furrow during cytokinesis, and the overexpression of C-terminal truncated mutant of radixin has been reported to induce bi-nucleation of human cultured cells [31,32], it

is speculated that ERMs are possibly involved in cytokinesis. However, in fruit fly cultured cells, which express only one member of ERMs, moesin, depletion of moesin does not block the progression of furrow ingression, but causes abnormal deformation of the plasma membrane during mitotic phase [33,34]. In mammalian cells, the involvement of ERMs in cell shape control during cytokinesis remains elusive. Moreover, it remains largely unknown whether the different groups of F-actin- and membrane-associated proteins are involved in the contractile ring-membrane linkage independent of each other, or if there is any interplay among them that coordinates the contractile ring-membrane interaction for proper cytokinesis control.

In this study, we investigated the intercellular dynamics and function of ERMs during cytokinesis in human cultured cells, focusing on the characteristics that distinguish ERMs from other cytokinesis-relevant proteins and the potential relationships among these membrane proteins.

Materials and methods

Cell culture

HeLa-Kyoto cell lines were cultured in Dulbecco's modified Eagle's medium (DMEM, Wako, Japan) supplemented with 10% foetal bovine serum and 1× antibiotic-antimycotic (Sigma-Aldrich, St. Louis, MO). A HeLa-Kyoto line stably expressing EGFP-myosin IIA was previously described [35]. The siRNAs used in this study are listed in Table S1. siRNA transfection was performed using Lipofectamine RNAiMAX (Thermo Fisher Scientific, Waltham, MA).

Plasmid construction and DNA transfection

The plasmid vectors constructed in this study are listed in Table S2. pEGFP-C3-myosin IIA [36] and pEGFP-C1-PLCd-PH [37] were purchased from Addgene (plasmid #11347 and #21179, respectively). The expression vector encoding GFP-ROCK II [38] or Lifeact-GFP was a kind gift from Dr. Kenji Fukasawa (Moffitt Cancer Center) or Dr. Shin-ichiro Kojima (Gakushuin Univeristy), respectively. DNA transfection was performed using JetPEI (Polyplus-transfection, Illkirch, France).

Immunofluorescence staining

For the immunostaining, cells were fixed with 3.2% paraformaldehyde in phosphate-buffered saline [PBS] for 10 min and permeabilized with 0.5% Triton-X100 in PBS supplemented with 0.1 M glycine [GPBS] for 10 min at 25˚C. For immunostaining of Rho, the cells were fixed with pre-chilled 10% trichloroacetic acid [TCA] on ice for 15 min [39], followed by permeabilization with 0.5% Triton-X100 in GPBS for 5 min at 25˚C. The fixed cells were incubated with the primary antibodies overnight at 4˚C, washed three times with PBS, and incubated with the secondary antibodies for 1 h at 37˚C. To stain chromosomes, DAPI (Dojindo, Kumamoto, Japan) was used at a final concentration of 1.0 μg/mL.

Immunoblotting

For immunoblotting, proteins separated by SDS-PAGE were transferred on to Immun-Blot PVDF

membrane (Bio-Rad, Hercules, CA). The blotted membranes were blocked with 0.3% skim milk in TTBS (50 mM Tris, 138 mM NaCl, 2.7 mM KCl, and 0.1% Tween 20), incubated with the primary antibodies overnight at 4˚C or for 1h at 37˚C, and incubated with the secondary antibodies for 30 min at 37˚C. Each step was followed by 3 washes with TTBS. For signal detection, the ezWestLumi plus ECL Substrate (ATTO, Tokyo, Japan) and a LuminoGraph II chemiluminescent imaging system (ATTO) were used.

Antibodies

Rat anti-α-tubulin (YOL1/34, EMD Millipore, Temecula, CA; 1:500 for IB), rat anti-GFP (GF090R, Nacalai, Kyoto, Japan; 1: 1000 for IB), goat anti-anillin (sc-54859, Santa Cruz Biotechnology, Dallas, TX; 1:500 for IF), rabbit anti-anillin (A301-405A, Bethyl Laboratories, Montgomery, TX; 1:50 for IB), mouse anti-ezrin (sc-58758, Santa Cruz Biotechnology; 1:100 for IF and 1:100 for IB), rabbit anti-radixin (EP1862Y, GeneTex, Irvine, CA; 1:200 for IF and 1:10000 for IB), rabbit anti-moesin (3150, Cell Signaling Technology, Danvers, MA; 1:300 for IF and 1:1000 for IB), rabbit anti-supervillin (NBP1-90363, Novus Biotechnologicals, Littleton, CO; 1:200 for IF and 1:500 for IB), mouse anti-RhoA (sc-418, Santa Cruz Biotechnology; 1:100 for IF), rabbit anti-RhoA, B, C (EPR18299, Abcam Cambridge, United Kingdom; 1: 500 for IF), rabbit anti-myosin IIA (a gift from Dr. K. Owaribe; 1:1000 for IF) [35], mouse anti-MLKP1 (a gift from Dr. K. Yoda; 1: 2 for IF) [35], and fluorescence- or horseradish peroxidase-conjugated secondary antibodies (Jackson ImmunoResearch Laboratories, West Grove, PA; 1:1000 for IF and IB) were purchased from the suppliers and used at the dilutions as indicated.

Depletion and visualization of cholesterol, or neomycin treatment

For cholesterol depletion, cells were treated with 10 or 20 mg/mL methyl-β-cyclodextrin (MβCD, Sigma-Aldrich) for more than 30 min at 37˚C. The visualization of cholesterol was performed using Cholesterol cell based detection assay kit (Cayman Chemical Company, Ann Arbor, MI) according to the manufacture's instruction. For neomycin treatment, cells were treated with 5 mM neomycin sulfate (Nacalai) for 17-18 h at 37˚C before cell fixation.

Cell imaging

Cells were observed under a TE2000 microscope (Nikon, Japan) equipped with a ×60 1.4 NA Plan-Apochromatic, a CSU-X1 confocal unit (Yokogawa, Tokyo, Japan), and an iXon3 electron multiplier-charge coupled device (EMCCD) camera (Andor, Belfast, United Kingdom) or ORCA-ER CCD camera (Hamamatsu Photonics, Hamamatsu, Japan). Image acquisition was controlled by μManager (Open Imaging). Transmission electron microscopy (TEM) was performed as previously described [40].

Image analyses

Quantification of fluorescence intensities by microscopy was performed using ImageJ (National Institutes of Health, Bethesda, MD). The quantification of the distribution of the GFP-tagged proteins along the cortex was conducted as follows. For control cells, the time frames of live cell images in which the furrow widths became below 5 μm were selected for analyses. For analysing anillin-depleted cells, we selected the time frames in which the area ratio of smaller to larger daughter cells fell within the range of

0.25 to 0.5, during which RLC-mCherry was fully delocalized from the equatorial furrow to the polar cortex. Line profiles along the cell cortex were taken from one cell pole to the opposite pole. For direct comparison among different samples, the pole-to-pole lengths of the line profiles were standardized to an arbitrary unit. The intensities of line profiles were also standardized after subtracting the cytoplasmic background, so that integral value of each line profile equals to 1. For line profiles in fixed cells, we chose the dividing cells with furrow width ranging from 10 to 5 μm (Fig. 3B, 4C, 6B, and S3G) or 14 to 4 μm (Fig. 4G), in which ezrin fully accumulated to the furrow in unperturbed condition. On the other hand, since depletion of MKLP1 severely blocked furrow ingression and precluded measurements of the cells with these ranges of furrow width, we analysed earlier stage of cytokinesis (with furrow width ranging from 15 and 10 μm) in Fig. 3E. After subtracting the cytoplasmic background, the line profile intensities were standardized to the average intensity at the cell equator in control cells. Kymographs in Fig. S1D were made using the Straighten plugin of ImageJ.

Results

ERMs are stably associated with the cleavage furrow membrane but not with the contractile ring

To gain insight into the organization of cytoskeleton-membrane interface during cytokinesis in the absence of anillin, we first tested the dynamics of the contractile ring and cytokinesis-relevant membrane domain, using mCherry-tagged myosin regulatory light chain (RLC) and GFP-tagged PLCδ-PH domain (as a PIP2 marker), respectively, in control and anillin-depleted HeLa cells (Fig. 1A, B, S1A and B). RLC-mCherry and GFP-PLCδ-PH co-localized at the cell equator in control cells [41]. In contrast, RLC-mCherry was frequently delocalized from the cell equator to the pole, resulting in oscillatory contraction of the polar cortex in anillin-depleted cells (Fig. 1A and Movie 1; see also Fig. 5D) [11,12]. During the oscillatory motion, RLC-mCherry co-localized with the F-actin structure visualized by lifeact-GFP, suggesting that RLC-mCherry reliably labels the contractile ring cytoskeleton even in this perturbed condition (Fig. S1C and D). During the oscillatory polar contraction in anillin-depleted cells, a large amount of GFP-PLCδ-PH was delocalized from the furrow and moved along the cortex together with the delocalized contractile ring, while the rest remain associated with the equatorial furrow region until the furrow regressed.

We next tested the dynamics of ezrin and supervillin during cytokinesis in control and anillin-depleted cells, using their GFP-tagged chimeras that were co-expressed with RLC-mCherry (Fig. 1A, B, and S1B). Both ezrin-GFP and GFP-supervillin localized to the cell equator in control cells. However, upon delocalization of the contractile ring in anillin-depleted cells, these two proteins showed notably distinct dynamics: While GFP-supervillin was delocalized from the equatorial membrane to cell poles along with the contractile ring cytoskeleton, most of the ezrin-GFP remained associated with the cleavage furrow at the cell equator and was dissociated from the contractile ring (Fig. 1A, and Movie 2 and 3). We also

noticed that a small portion of ezrin-GFP transiently accumulated at the polar region and co-localized with RLC-mCherry only during the gross contraction of the polar cortex in these anillin-depleted cells (Fig. 1A, enlarged polar cortex images). Quantification of the signal distributions of ezrin-GFP and GFP-supervillin along the cell membrane confirmed the striking difference in their distributions upon the delocalization of the contractile ring in anillin-depleted cells (Fig. 1B). An immunostaining analysis also revealed the preferential association of supervillin or ERMs with the contractile ring cytoskeleton or the cleavage furrow membrane, respectively, in anillin-depleted cells (Fig. S1E and F). To specify the protein domain responsible for the characteristic distribution of ezrin in anillin-depleted cells, we tested the dynamics of GFP-tagged truncated mutants of ezrin (Fig. 2A and B, and S1B) [22]. The localization of the GFP-tagged FERM domain of ezrin (ezrin-FERM-GFP; 1-309 a.a.) was similar to that of full-length protein both before and after the delocalization of the contractile ring cytoskeleton in anillin-depleted cells (Fig. 2A and B). In contrast, the GFP-tagged C-terminal half of ezrin (ezrin-C-term-GFP; 296-586 a.a.) that contains the actin-binding domain predominantly distributed in the cytoplasm while its association with the cell cortex was barely visible both in control and anillin-depleted cells (Fig. 2A). Therefore, the characteristic localization of ezrin in anillin-depleted cells seems due to its association with the membrane rather than the cytoskeleton, which is consistent with reportedlocalizations of the radixin truncated mutants in unperturbed cells [32]. These results indicate that ERMs have poor association with the contractile ring cytoskeleton and that their recruitment to the cleavage furrow is achieved through their association with the equatorial membrane domain.

The accumulation of ezrin at the cleavage furrow requires cholesterol but not RhoA

We next addressed what determines the characteristic localization of ERMs at the cleavage furrow. The localization of ERMs in anillin-depleted cells resembled those of exogenously expressed *C. elegans* Rho1 or a RhoA-binding domain of anillin in a previous study [12], or another RhoA effector, ROCK II/Rho-kinase2 (Fig. S2A and B). Since RhoA signaling is involved in the recruitment of ERMs to the plasma membrane [27,28,42], we next tested the potential contribution of RhoA to the accumulation of ERMs at the cleavage furrow. Depletion of RhoA by RNAi efficiently diminished immunostaining signal of RhoA at the cleavage furrow (Fig. 3A and B). In contrast, immunostaining signal of ezrin at the cleavage furrow remained unchanged in RhoA-depleted cells when compared to control cells (Fig. 3A and B). To exclude the possible involvement of other Rho homologues (RhoB and RhoC) in recruitment of ERMs at the cleavage furrow, we also depleted an upstream factor of Rho, MKLP1, which is required for localization of all Rho homologues at the furrow [43]. Depletion of MKLP1 indeed severely diminished immunostaining signal of the antibody against all Rho homologues at the cleavage furrow (Fig. 3C-E). Since depletion of MKLP1 blocked full ingression of the cleavage furrow, we compared the accumulation of ezrin in the early phase of cytokinesis between control and MKLP1-depleted cells (see *Materials and methods*). Although we observed the trend of broadening of ezrin staining upon MKLP1 depletion, there was no statistically significant difference in the distribution of ezrin between control and MKLP1-depleted cells (Fig. 3D and E). These results suggest that the association of ERMs with the cell equator is mediated through a mechanism distinct from the Rho-mediated signaling cascade.

Previous studies have reported the association of ERMs with microvilli at the cleavage furrow [31,44]. However, it is unclear whether the association of ERMs with microvilli is prerequisite for their accumulation at the cleavage furrow, especially considering that ERMs also have the ability to associate with other membrane structures besides microvilli [32,45,46]. To gain insight into the causal relationship between the association of ERMs with microvilli and their localization at the cleavage furrow, we tested the effect of microvilli perturbation on the spatial distribution of ERMs. We treated dividing cells with methyl-b-cyclodextrin (MbCD), which has been reported to deplete cholesterol and severely impair microvilli formation in interphase epithelial cells [47,48]. In control untreated cells, the cleavage furrow was preferentially stained by a cholesterol-binding fluorescent compound filipin [49], but this filipin staining was drastically diminished in MbCD treated cells (Fig. S2C and D). TEM analysis revealed severe perturbation of the organization of microvilli at the cleavage furrow in MbCD treated cells (Fig. 4A), and these cells also drastically mislocalized ezrin to the polar cortex (Fig. 4B and C). Line profiles along the cortex showed a significant reduction in accumulation of ezrin at the equatorial region (Fig. 4C). Notably, MbCD treatment resulted in only mild reduction of the equatorial accumulation of anillin, or RhoA, and gross mis-localization of these factors was never observed (Fig. 4B and C). This suggests that the mechanisms that accumulate these cytokinesis-relevant membrane proteins were preserved in this experimental condition, and that the prerequisite for the localization of ERMs at the cleavage furrow is clearly distinct from those of these other membrane proteins.

We also tested the effect of MbCD treatment on the localization of PIP2, which also accumulates at microvilli and is required for membrane association of ERMs and microvilli formation [27,29,50,51], using GFP-PLCd-PH co-expressed with ezrin-mCherry (Fig. 4D and E). GFP-PLCd-PH and ezrin-mCherry were severely delocalized from the equatorial furrow in a substantial number of MbCD treated cells (12 out of 29 cells), but never in untreated cells (0 out 20 cells). Interestingly, even in these cases, the distribution patterns of these two markers along the cell membrane still coincided strikingly (Fig. 4E), suggesting that ezrin continues to associate with PIP2 at the cell membrane in the absence of cholesterol. Consistent with the persistent co-localization of ezrin with PIP2, treatment of the cells with neomycin, which binds to PIP2 and block the interaction between PIP2 and PIP2-binding proteins [52], significantly reduced the amount of ezrin at the cleavage furrow compared to untreated control (Fig. 4F and G). These results suggest that the accumulation of ERMs at the cleavage furrow is predominantly dependent on their association with microvilli there.

ERMs engage in furrowing activity in anillin- and supervillin-co-depletion background

Following the finding of the characteristic dynamics and localization mechanism of ERMs at the cleavage furrow, we next addressed whether ERMs play any role, either singly or in cooperation with other cytokinesis-relevant proteins, in controlling cell shape during cytokinesis. For that purpose, ERMs were depleted by RNAi, in combination with depletion of anillin and/or supervillin in HeLa cells expressing GFP-myosin IIA, and the furrow ingression during cytokinesis in these cells was monitored by live

imaging. To minimize the possibility of blunting of RNAi response by combined use of siRNAs for multiple targets, we used siRNAs at relatively low concentration (5 nM each). Each target protein was efficiently depleted in this experimental condition (Fig. 5A). Depletion of ERMs did not have a gross influence on the progression of furrow ingression (Fig. 5B). We did not find a significant change in the kinetics of furrow ingression even when cells were treated with 10-fold higher concentration of the ERMs-targeting siRNAs (Fig. S3A). Therefore, ERMs do not seem to make significant contribution to the progression of furrow ingression during cytokinesis in HeLa cells.

On the other hand, depletion of anillin or supervillin significantly slowed furrow ingression when compared to control cells (Fig. 5B). Interestingly, co-depletion of supervillin and anillin resulted in significant acceleration of furrow ingression when compared to anillin depletion alone. However, this acceleration of furrow ingression was suppressed when ERMs were co-depleted along with anillin and supervillin (Fig. 5B). Similar effect of ERMs depletion was also observed using another set of ERM-targeting siRNAs (Fig. S3B and C). This result suggests that ERMs are required for furrow ingression in absence of anillin and supervillin. Besides the kinetics of furrow ingression, we also noticed that co-depletion of ERMs with anillin drastically suppressed the oscillatory contraction of the polar cortex caused by anillin single depletion, suggesting their involvement in the polar cortical activity during cytokinesis (Fig. 5C and D). To exclude the possibility that ERMs depletion changed the furrowing kinetics merely through the suppression of irregular polar contraction in anillin and supervillin-co-depleted cells, we also compared the furrowing kinetics among these RNAi conditions only using the data from the cells that did not show the oscillatory polar contraction (Fig. S3D). Even in this analysiscondition, ERM depletion delayed the furrow ingression in anillin and supervillin co-depletion background, suggesting the direct involvement of ERMs in furrow ingression activity in this experimental background.

Anillin and supervillin limit the access of ezrin to the cleavage furrow

To understand the mechanism underlying the increased contribution of ERMs to furrow ingression in the absence of supervillin and anillin, we next tested the effects of anillin and/or supervillin depletion on the distribution of ezrin in dividing cells using immunostaining (Fig. 6A, B, S3E, F, and G). In cells depleted of either anillin or supervillin, the amount of ezrin accumulated at the cleavage furrow was significantly higher than that in control cells (Fig. 6B, and S3G), while the expression levels of ERMs remained unchanged (Fig. 5A, and S3E). Simultaneous depletion of anillin and supervillin further increased the accumulation of ezrin at the cleavage furrow, resulting in greater than two-fold increase in intensity of ezrin immunostaining at the center of the cleavage furrow in anillin- and supervillin-co-depleted cells compared to those in control cells (Fig. 6B, and S3G). This suggests that anillin and supervillin usually limit the access of ERMs to the cleavage furrow, and thus limit the contribution of ERMs to furrow ingression activity during cytokinesis.

Discussion

The identities of the molecular entities of the cytoskeleton-membrane cross linkers that play pivotal roles in the regulation of the cortical contractile activities and the plasma membrane deformation during cytokinesis remain largely elusive. Among numerous actin-membrane-binding proteins, ERMs show prominent accumulation at the equatorial membrane in dividing cells, but their roles in regulation of cytokinesis progression are not known in mammalian cells. Our results provide novel insights into the characteristic dynamics of ERMs and their contribution to cortical contractile activities during cytokinesis in mammalian cells.

While recent studies using fruit fly cells have revealed the pivotal role of spatially controlled dephosphorylation of moesin in its exclusion from the polar cortex during anaphase [1,53,54], the molecular mechanism that governs the accumulation of ERMs at the cell equator during cytokinesis remains unknown. A distinctive feature of ERMs localization is their association with microvilli at the cleavage furrow [31,44], but it has been unclear what fraction of ERMs there are associated with microvilli. We found that either MbCD or neomycin treatment lead to a drastic reduction in the accumulation of ezrin at the cleavage furrow. Because these compounds have been shown to disorganize microvilli in interphase and MbCD also severely impaired microvilli formation in dividing cells (Fig. 4A) [29,47,51], microvilli are likely to be primary scaffolds for ERMs accumulation at the cleavage furrow. On the other hand, essential cytokinesis-relevant membrane proteins, such as RhoA and anillin remained localized at the cleavage furrow in MbCD treated cell, and oppositely, substantial inhibition of the Rho-activating pathway did not largely affect the accumulation of ezrin at the cleavage furrow. Therefore, the localization of ERMs at the cleavage furrow is regulated separately from the Rho-mediated pathway that plays a central role in spatial reorganization of the contractile ring formation. In this regard, the poor accumulation of the C-terminus truncated forms of ERMs at the equatorial cortex (Fig. 2A) [32] and the lack of continuous association of full length ERMs with delocalized contractile ring in anillin-depleted cells indicate their limited association with the contractile ring cytoskeleton. Consistent with their poor association with the contractile ring, our functional analyses indicate that ERMs have little contribution to the progression of furrow ingression during cytokinesis. This is also consistent with the lack of increase in bi-nucleated cells upon gene silencing of ERMs in a previous study [55]. On the other hand, ERMs transiently associated with the cellular polar cortex and profoundly contributed to the oscillatory contraction of cell poles that was caused in the absence of anillin. This suggests that, during cytokinetic phase, ERMs have the potential to be actively involved in the cytoskeleton-membrane association and mediate cortical contractile activities. Notably, when anillin and supervillin were co-depleted, the association of ezrin with the cleavage furrow drastically increased and ERMs made significant contributions to furrow ingression activity. This indicates a backup function of ERMs in the regulation of furrow ingression. However, the up-regulated association of ezrin with the contractile ring did not sufficiently suppress the furrow ingression defect brought about by perturbation of the other membrane proteins, suggesting that it cannot singly support the whole process of cytokinesis. This may be because ERMs are acquired upon the transition to multicellularity in metazoa and are primarily designed to mediate cellular processes such as cell-cell and cell-substrate communications. The drastic

change in the access of ERMs to the cleavage furrow upon co-depletion of supervillin and anillin also implies a mechanism that preferentially recruits cytokinesis-relevant proteins, such as anillin and supervillin, to the division site over other non- or less relevant proteins, such as ERMs. Since there are numerous actin-membrane-associated proteins filling the cytoskeleton-membrane interface, such selective sorting would be necessary for cytokinesis-relevant proteins to make their full contribution to cytokinesisregulation. Further analyses of the molecular and structural basis of the preferential association of the cytokinesis-relevant proteins with the cell division site over other proteins would be useful to elucidate the whole picture of the fine-tuning of cytoskeleton-membrane interaction in control of cell shape changes during cytokinesis in animal cells.

Acknowledgments

We are grateful to Mithilesh Mishra, Sarada Bulchand, for valuable comments on the draft of this paper, Kan Yaguchi for technical assistance, Issei Mabuchi, Akira Kitamura, Masataka Kinjo for useful discussions, to the members of the Faculty of Advanced Life Science and Nikon Imaging Center at Hokkaido University for the use of their devices, and to Kenji Fukasawa, Gohta Goshima, Shin-ichiro Kojima, Katsushi Owaribe, and Yoshiaki Hirako for sharing their reagents. This work was supported by the Akiyama Life Science Foundation, the Inamori Foundation, the Nakajima Foundation, the Suhara Memorial Foundation, the Takeda Science Foundation, and the Cooperative Research Program of "Network Joint Research Center for Material and Devices" to R. U., and MEXT/JSPS KAKENHI (Grants Numbers 15K14501, and 17K15111 to R.U., and 15H05953 "Resonance Bio" to K.O. and T. N.).

Figure legends

Fig. 1: The cytoskeleton-membrane interface organization in anillin-depleted cells
(**A**) Live imaging of mock- or anillin-depleted HeLa cells transiently expressing GFP-PLCd-PH, GFP-supervillin, or ezrin-GFP (green) with myosin RLC-mCherry (magenta). Enlarged images of the polar region in the ezrin-GFP-expressing cell (indicated by a yellow inset) are shown at the bottom. Arrowheads: accumulation of the respective GFP-tagged proteins. Scale bars, 5 μm. (**B**) Top: Schematic images of line profiles along the cell cortex/membrane in control (left) and anillin-depleted cells in asymmetric shapes because of the contractile ring delocalization (right, magenta). Note that, in anillin-depleted cells, a time frame at which myosin signal fully localized to the pole was selected from each live cell image series, and that this does not represent the trend of the entire process of the oscillatory motion. For anillin-depleted cells, the line profiles were taken from the constricting pole (black arrowhead) to the expanding pole (while arrowhead). See *Materials and methods* for details of the quantification. Bottom: Quantification of the distribution of each fluorescence tagged protein along the cell cortex/membrane in control, or anillin-depleted cells after delocalization of the contractile ring. Mean ± SE of at least 10 line profiles from 5 cells from at least 3 independent experiments for each condition.

Fig. 2: Localization of GFP-tagged ezrin truncated mutants in anillin-depleted cells

(**A**) Live imaging of mock- or anillin-depleted HeLa cells transiently expressing GFP-tagged truncated mutants of ezrin with myosin RLC-mCherry. Scale bars, 5 μm. (**B**) Quantification of the distribution of the fluorescence tagged protein along the cell cortex/membrane in control, or anillin-depleted cells after delocalization of the contractile ring. Mean ± SE of at least 12 line profiles from 6 cells from 2 independent experiments for each condition. The quantification was not applicable to the C-terminal mutant because of its cytoplasmic distribution.

Fig. 3: Inhibition of Rho-activating pathway does not abolished ERM accumulation at the cleavage furrow

(**A**, **C**, **D**) Immunostaining of ezrin or RhoA (A), MKLP1 (C), or ezrin or all Rho homologues (D) in RNAi-treated cells. DNA was stained by DAPI (blue). Scale bars, 5 μm. (**B**, **E**) Quantification of immunostaining signals at the cleavage furrow in A, or D. Mean ± SE of at least 14 line profiles from 7 cells (B), or at least 34 line profiles from 17 cells (E) from 2 independent experiments for each condition. Asterisk indicates significant difference from control (at the cell equator; * $p < 10^{-7}$, *t*-test).

Fig. 4: The accumulation of ezrin at the cleavage furrow is dependent on cholesterol and PIP2

(**A**) TEM images of a control or a MbCD-treated dividing cell. Serially sectioned images of the cleavage furrow (boxes) at higher magnification are shown in lower panels. Arrows indicate microvilli. Severemicrovilli perturbation was observed in 4 of 4 MbCD-treated cells from 2 independent experiments, but none of 6 control cells from 3 independent experiments. (**B**) Immunostaining of ezrin, anillin, or RhoA in the cells treated with or without MbCD. (**C**) Line profiles of immunostaining intensity taken along the cell cortex in B. Mean ± SE of at least 20 line profiles from 10 cells from 2 independent experiments were analysed for each condition. Asterisks indicate significant differences from control (at the cell equator; * $p < 10^{-3}$, ** $p < 10^{-6}$, *t*-test). (**D**) Live imaging of the cells transiently expressing GFP-PLCd-PH (green) and ezrin-mCherry (magenta) that were treated with or without MbCD. (**E**) Representative examples of line profiles along the cortex in D. Line profiles taken from three different cells are shown for each condition. (**F**) Immunostaining of ezrin in the cells treated with or without 5 mM neomycin. Scale bars, 5 μm. (**G**) Line profiles of immunostaining intensity taken along thecell cortex in F. Mean ± SE of at least 12 line profiles from 6 cells from 2 independent experiments were analysed for each condition. Asterisk indicates significant difference from control (at the cell equator; * $p < 0.01$, *t*-test).

Figure 5: Effect of co-depletion of ERMs with other membrane proteins on cytokinesis

(**A**) Immunoblotting of ezrin, radixin, moesin, anillin, and supervillain in the RNAi-treated cells. a-tubulin was used as a loading control. Closed or open arrowhead indicates radixin or moesin-specific bands, respectively. (**B**) Time courses of cleavage furrow widths in live cell imaging of RNAi-treated GFP-myosin IIA cells. Mean ± SE of at least 14 cells from at least 2 independent experiments for each

condition. At 18 min after anaphase onset, furrow width was significantly wider in anillin, supervillin, and ERMs-co-depleted cells than in anillin and supervillin-co-depleted cells (* $p < 0.05$, *t*-test). (**C**) Live cell images of an anillin-depleted or an anillin- and ERMs-co-depleted cell expressing GFP-myosin IIA. Arrowheads indicate oscillatory contraction of the polar cortex. Time of anaphase onset was set as 0 min. Scale bar, 5 μm. (**D**) Frequency of oscillatory polar cortical contraction in the RNAi-treated GFP-myosin IIA cells. At least 22 cells from at least 2 independent experiments were analysed for each condition.

Figure 6: Enhanced association of ezrin with the cleavage furrow upon depletion of anillin and/or supervillin

(**A**) Immunostaining of ezrin in RNAi-treated cells. Scale bar, 5 μm. (**B**) Line profiles of immunostaining signals along the cell cortex in A. Mean ± SE of at least 20 line profiles from 10 cells from 2 independent experiments for each condition. Immunostaining signal of ezrin at the cell equator was significantly higher in the cells depleted of anillin and/or supervillin than in control cells ($p < 0.001$, *t*-test).

Figure S1: Localization of supervillin and ERMs in anillin-depleted cells

(**A**) Immunoblotting of anillin in the RNAi-treated cells. a-tubulin was used as a loading control. (**B**) Immunoblotting of GFP-tagged proteins transiently expressed in the experiments in Figure 1A, 2A, and S2A. (**C**) Live imaging of anillin-depleted HeLa cells transiently expressing Lifeact-GFP (green), and RLC-mCherry (magenta). The arrowhead indicates the original position of the cell equator. (**D**) Kymographs of RLC-mCherry and Lifeact-GFP taken along the cell cortex in C. Top: An example of regions of interest (ROIs) used for kymograph. (**E**) Immunostaining of supervillin, ezrin, moesin, or radixin in mock- or anillin-depleted GFP-myosin IIA (G-Myo)-expressing cells. DNA was stained by DAPI (blue). Scale bars, 5 μm. (**F**) Top: Schematic images of different classes of distribution patterns of myosin II and membrane proteins. Bottom: Frequencies of different classes of distribution patterns of supervillin, ERMs, and GFP-myosin IIA in C. At least 9 cells from 2 independent experiments were analysed for each condition.

Figure S2: Localization of different proteins and cholesterol in anillin-depleted cells

(**A**) Live imaging of mock- or anillin-depleted HeLa cells transiently expressing GFP-ROCK II, or GFP-anillin-C-terminal truncated mutant (green) with myosin RLC-mCherry (magenta). (**B**) Quantification of the distribution of each fluorescence tagged protein along the cell cortex/membrane in control, or anillin-depleted cells after delocalization of the contractile ring. Mean ± SE of at least 6 line profiles from 3 cells from at least 2 independent experiments for each condition. (**C**) Control or MbCD-treated, or mock- or anillin-depleted HeLa cells that were fixed and stained with filipin. Scale bars, 5 μm. (**D**) Quantification of the equatorial and polar cortical distribution of filipin staining in C. Mean ± SE of at least 16 cells from 2 independent experiments for each condition (*p* value of *t*-test). An example of ROIs used for the quantification is shown on top.

Figure S3: ERMs become involved in furrow ingression activity upon co-depletion of anillin and

supervillin

(**A**) Time courses of cleavage furrow widths in live cell imaging of RNAi-treated GFP-myosin IIA cells. Cells were treated with siRNA targeting luciferase (as negative control; 150 nM) or mixture of siRNAs targeting ezrin, radixin, or moesin (50 nM each). Mean ± SE of at least 11 cells from 2 independent experiments for each condition. (**B**, **E**) Immunoblotting of ezrin, radixin, moesin, anillin, and supervillin in the RNAi-treated cells. a-tubulin was used as a loading control. Closed or open arrowheads indicate radixin or moesin-specific bands, respectively. (**C**) Time courses of cleavage furrow widths in live cell imaging of GFP-myosin IIA cells treated with a different set of siRNAs against ERMs from Fig. 4B and S3A. Mean ± SE of at least 5 cells from 2 independent experiments for each condition. At 18 min after anaphase onset, furrow width was significantly wider in anillin, supervillin, and ERMs-co-depleted cells than in anillin and supervillin-co-depleted cells (* $p < 10^{-5}$, *t*-test). (**D**) Time courses of cleavage furrow widths in live cell imaging of anillin-depleted, anillin and supervillin co-depleted, or anillin, supervillin, and ERMs-co-depleted cells that did not show oscillatory polar contraction in Fig. 5B. The data of the cells without oscillatory polar contraction were selected for reanalysis from the same dataset used in Fig. 5B. Mean ± SE of at least 13 cells from at least 3 independent experiments for each condition. At 18 min after anaphase onset, furrow width was significantly wider in anillin, supervillin, and ERMs-co-depleted cells than in anillin and supervillin-co-depleted cells (* $p < 0.01$, *t*-test). (**F**) Immunostaining of ezrin (green) and myosin IIA (magenta) in RNAi-treated cells. Scale bar, 5 μm. (**G**) Line profiles of immunostaining signals along the cell cortex in F. Mean ± SE of at least 18 line profiles from 9 cells from 2 independent experiments for each condition. Immunostaining signal of ezrin at the cell equator was significantly higher in the cells depleted of anillin ($p < 0.05$, *t*-test), or anillin and supervillin ($p < 10^{-5}$, *t*-test) than in control cells.

Movie 1: Live imaging of anillin-depleted HeLa cells transiently expressing GFP-PLCd-PH (green) with myosin RLC-mCherry (magenta). Field of view is 36 μm × 36 μm.

Movie 2: Live imaging of anillin-depleted HeLa cells transiently expressingGFP-supervillin (green) with myosin RLC-mCherry (magenta). Field of view is 36 μm × 36 μm.

Movie 3: Live imaging of anillin-depleted HeLa cells transiently expressing ezrin-GFP (green) with myosin RLC-mCherry (magenta). Field of view is 36 μm × 36 μm.

References

[1] Rodrigues, N.T.L., Lekomtsev, S., Jananji, S., Kriston-Vizi, J., Hickson, G.R.X. and Baum, B. (2015). Kinetochore-localized PP1-Sds22 couples chromosome segregation to polar relaxation. Nature 524, 489-492.

[2] Sedzinski, J., Biro, M., Oswald, A., Tinevez, J.-Y., Salbreux, G. and Paluch, E. (2011). Polar actomyosin contractility destabilizes the position of the cytokinetic furrow.

Nature 476, 462-466.
[3] Kotadia, S., Montembault, E., Sullivan, W. and Royou, A. (2012). Cell elongation is an adaptive response for clearing long chromatid arms from the cleavage plane. The Journal of Cell Biology 199, 745-753.
[4] Schroeder, T.E. (1970). Thecontractile ring. I. Fine structure of dividing mammalian (HeLa) cells and the effects of cytochalasin B. Z Zellforsch Mikrosk Anat 109, 431-49.
[5] Schroeder, T.E. (1972). THE CONTRACTILE RING : II. Determining its Brief Existence, Volumetric Changes, and Vital Role in Cleaving Arbacia Eggs. The Journal of Cell Biology 53, 419-434.
[6] Saarikangas, J., Zhao, H. and Lappalainen, P. (2010). Regulation of the actin cytoskeleton-plasma membrane interplay by phosphoinositides. Physiol Rev 90, 259-89.
[7] Bezanilla, M., Gladfelter, A.S., Kovar, D.R. and Lee, W.-L. (2015). Cytoskeletal dynamics: A view from the membrane. The Journal of Cell Biology 209, 329-337.
[8] Field, C.M. and Alberts, B.M. (1995). Anillin, a contractile ring protein that cycles from the nucleus to the cell cortex. The Journal of Cell Biology 131, 165-178.
[9] Giansanti, M.G., Bonaccorsi, S. and Gatti, M. (1999). The role of anillin in meiotic cytokinesis of Drosophila males. Journal of Cell Science 112, 2323-2334.
[10] Oegema, K., Savoian, M.S., Mitchison, T.J. and Field, C.M. (2000). Functional analysis of a human homologue of the Drosophila actin binding protein anillin suggests a role in cytokinesis. J Cell Biol 150, 539-52.
[11] Straight, A.F., Field, C.M. and Mitchison, T.J. (2005). Anillin binds nonmuscle myosin II and regulates the contractile ring. Mol Biol Cell 16, 193-201.
[12] Piekny, A.J. and Glotzer, M. (2008). Anillin is a scaffold protein that links RhoA, actin, and myosin during cytokinesis. Curr Biol 18, 30-6.
[13] Liu, J., Fairn, Gregory D., Ceccarelli, Derek F., Sicheri, F. and Wilde, A. (2012). Cleavage Furrow Organization Requires PIP2-Mediated Recruitment of Anillin. Current Biology 22, 64-69.
[14] Smith, T.C. et al. (2013). Supervillin binding to myosin II and synergism with anillin are required for cytokinesis. Molecular Biology of the Cell 24, 3603-3619.
[15] Chen, Y. et al. (2003). F-actin and Myosin II Binding Domains in Supervillin. Journal of Biological Chemistry 278, 46094-46106.
[16] Pestonjamasp, K.N., Pope, R.K., Wulfkuhle, J.D. and Luna, E.J. (1997). Supervillin (p205): A Novel Membrane-associated, F-Actin–binding Protein in the Villin/Gelsolin Superfamily. The Journal of Cell Biology 139, 1255-1269.
[17] Pestonjamasp, K., Amieva, M.R., Strassel, C.P., Nauseef, W.M., Furthmayr, H. and Luna, E.J. (1995). Moesin, ezrin, andp205 are actin-binding proteins associated with neutrophil plasma membranes. Molecular Biology of the Cell 6, 247-259.
[18] Hasegawa, H. et al. (2013). The role of PLK1-phosphorylated SVIL in myosin II activation and cytokinetic furrowing. Journal of Cell Science 126, 3627-3637.
[19] Smith, T.C., Fang, Z. and Luna, E.J. (2010). Novel interactors and a role for supervillin in early cytokinesis. Cytoskeleton (Hoboken) 67, 346-64.
[20] Tsukita, S., Yonemura, S. and Tsukita, S. (1997). ERM proteins: head-to-tail regulation of actin-plasma membrane interaction. Trends in Biochemical Sciences 22, 53-58.
[21] Tsukita, S. and Yonemura, S. (1999). Cortical actin organization: lessons from ERM (ezrin/radixin/moesin) proteins. J Biol Chem 274, 34507-10.
[22] Algrain, M., Turunen, O., Vaheri, A., Louvard, D. and Arpin, M. (1993). Ezrin contains cytoskeleton and membrane binding domains accounting for its proposed role as a membrane-cytoskeletal linker. The Journal of Cell Biology 120, 129-139.
[23] Fehon, R.G., McClatchey, A.I. and Bretscher, A. (2010). Organizing the cell cortex:

the role of ERM proteins. Nat Rev Mol Cell Biol 11, 276-87.
[24] Neisch, A.L. and Fehon, R.G. (2011). Ezrin, Radixin and Moesin: key regulators of membrane-cortex interactions and signaling. Curr Opin Cell Biol 23, 377-82.
[25] Arpin, M., Chirivino, D., Naba, A. and Zwaenepoel, I. (2011). Emerging role for ERM proteins in cell adhesion and migration. Cell Adh Migr 5, 199-206.
[26] Gary, R. and Bretscher, A. (1995). Ezrin self-association involves binding of an N-terminal domain to a normally masked C-terminal domain that includes the F-actin binding site. Mol Biol Cell 6, 1061-75.
[27] Hirao, M. et al. (1996). Regulation mechanism of ERM (ezrin/radixin/moesin) protein/plasma membrane association: possible involvement of phosphatidylinositol turnover and Rho-dependent signaling pathway. J Cell Biol 135, 37-51.
[28] Matsui, T., Yonemura, S., Tsukita, S. and Tsukita, S. (1999). Activation of ERM proteins in vivo by Rho involves phosphatidyl-inositol 4-phosphate 5-kinase and not ROCK kinases. Curr Biol 9, 1259-62.
[29] Yonemura, S., Matsui, T., Tsukita, S. and Tsukita, S. (2002). Rho-dependent and -independent activation mechanisms of ezrin/radixin/moesin proteins: an essential role for polyphosphoinositides in vivo. J Cell Sci 115, 2569-80.
[30] Fievet, B.T., Gautreau, A., Roy, C., DelMaestro, L., Mangeat, P., Louvard, D. and Arpin, M. (2004). Phosphoinositide binding and phosphorylation act sequentially in the activation mechanism of ezrin. J Cell Biol 164, 653-9.
[31] Sato, N., Yonemura, S., Obinata, T., Tsukita, S. and Tsukita, S. (1991). Radixin, a barbed end-capping actin-modulating protein, is concentrated at the cleavage furrow during cytokinesis. The Journal of Cell Biology 113, 321-330.
[32] Henry, M.D., Gonzalez Agosti, C. and Solomon, F. (1995). Molecular dissection of radixin: distinct and interdependent functions of the amino- and carboxy-terminal domains. The Journal of Cell Biology 129, 1007-1022.
[33] Carreno, S., Kouranti, I., Glusman, E.S., Fuller, M.T., Echard, A. and Payre, F. (2008). Moesin and its activating kinase Slik are required for cortical stability and microtubule organization in mitotic cells. The Journal of Cell Biology 180, 739-746.
[34] Kunda, P., Pelling, A.E., Liu, T. and Baum, B. (2008). Moesin Controls Cortical Rigidity, Cell Rounding, and Spindle Morphogenesis during Mitosis. Current Biology 18, 91-101.
[35] Uehara, R., Kamasaki, T., Hiruma, S., Poser, I., Yoda, K., Yajima, J., Gerlich, D.W. and Goshima, G. (2016). Augmin shapes the anaphase spindle for efficient cytokinetic furrow ingression and abscission. Mol Biol Cell 27, 812-27.
[36] Wei, Q. and Adelstein, R.S. (2000). Conditional expression of a truncated fragment of nonmuscle myosin II-A alters cell shape but not cytokinesis in HeLa cells. Mol Biol Cell 11, 3617-27.
[37] Stauffer, T.P., Ahn, S. and Meyer, T. (1998). Receptor-induced transient reduction in plasma membrane PtdIns(4,5)P2 concentration monitored in living cells. Current Biology 8, 343-346.
[38] Ma, Z., Kanai, M., Kawamura, K., Kaibuchi, K., Ye, K. and Fukasawa, K. (2006). Interaction between ROCK II and nucleophosmin/B23 in the regulation of centrosome duplication. Mol Cell Biol 26, 9016-34.
[39] Nishimura, Y. and Yonemura, S. (2006). Centralspindlin regulates ECT2 and RhoA accumulation at the equatorial cortex during cytokinesis. J Cell Sci 119, 104-14.
[40] Kon, S. et al. (2017). Cell competition with normal epithelial cells promotes apical extrusion of transformed cells through metabolic changes. Nat Cell Biol 19, 530-541.
[41] Field, S.J., Madson, N., Kerr, M.L., Galbraith, K.A.A., Kennedy, C.E., Tahiliani, M., Wilkins, A. and Cantley, L.C. (2005). PtdIns(4,5)P2 Functions at the Cleavage Furrow during Cytokinesis. Current Biology 15, 1407-1412.

[42] Shaw, R.J., Henry, M., Solomon, F. and Jacks, T. (1998). RhoA-dependent phosphorylation and relocalization of ERM proteins into apical membrane/actin protrusions in fibroblasts. Mol Biol Cell9, 403-19.

[43] Kamijo, K., Ohara, N., Abe, M., Uchimura, T., Hosoya, H., Lee, J.S. and Miki, T. (2006). Dissecting the role of Rho-mediated signaling in contractile ring formation. Mol Biol Cell 17, 43-55.

[44] Yonemura, S., Nagafuchi, A., Sato, N. and Tsukita, S. (1993). Concentration of an integral membrane protein, CD43 (leukosialin, sialophorin), in the cleavage furrow through the interaction of its cytoplasmic domain with actin-based cytoskeletons. The Journal of Cell Biology 120, 437-449.

[45] Tsukita, S., Hieda, Y. and Tsukita, S. (1989). A new 82-kD barbed end-capping protein (radixin) localized in the cell-to-cell adherens junction: purification and characterization. J Cell Biol 108, 2369-82.

[46] Hayashi, K., Yonemura, S., Matsui, T. and Tsukita, S. (1999). Immunofluorescence detection of ezrin/radixin/moesin (ERM) proteins with their carboxyl-terminal threonine phosphorylated in cultured cells and tissues. J Cell Sci 112 (Pt 8), 1149-58.

[47] Marzesco, A.M., Wilsch-Brauninger, M., Dubreuil, V., Janich, P., Langenfeld, K., Thiele, C., Huttner, W.B. and Corbeil, D. (2009). Release of extracellular membrane vesicles from microvilli of epithelial cells is enhanced by depleting membrane cholesterol. FEBS Lett 583, 897-902.

[48] Ilangumaran, S. and Hoessli, D.C. (1998). Effects of cholesterol depletion by cyclodextrin on the sphingolipid microdomains of the plasma membrane. Biochemical Journal 335, 433-440.

[49] Drabikowski, W., Łagwińska, E. and Sarzała, M.G. (1973). Filipin as a fluorescent probe for the location of cholesterol in the membranes of fragmented sarcoplasmic reticulum. Biochimica et Biophysica Acta (BBA) - Biomembranes 291, 61-70.

[50] Heiska, L., Alfthan, K., Gronholm, M., Vilja, P., Vaheri, A. and Carpen, O. (1998). Association of ezrin with intercellular adhesion molecule-1 and -2 (ICAM-1 and ICAM-2). Regulation by phosphatidylinositol 4, 5-bisphosphate. J Biol Chem 273, 21893-900.

[51] Ikenouchi, J., Hirata, M., Yonemura, S. and Umeda, M. (2013). Sphingomyelin clustering is essential for the formation of microvilli. J Cell Sci 126, 3585-92.

[52] Zhang, J., Kong, C., Xie, H., McPherson, P.S., Grinstein, S. and Trimble, W.S. (1999). Phosphatidylinositol polyphosphate binding to the mammalian septin H5 is modulated by GTP. Curr Biol 9, 1458-67.

[53] Roubinet, C., Decelle, B., Chicanne, G., Dorn, J.F., Payrastre, B., Payre, F. and Carreno, S. (2011). Molecular networks linked by Moesin drive remodeling of the cell cortex during mitosis. The Journal of Cell Biology 195, 99-112.

[54] Kunda, P., Rodrigues, N.T., Moeendarbary,E., Liu, T., Ivetic, A., Charras, G. and Baum, B. (2012). PP1-mediated moesin dephosphorylation couples polar relaxation to mitotic exit. Curr Biol 22, 231-6.

[55] Takeuchi, K., Sato, N., Kasahara, H., Funayama, N., Nagafuchi, A., Yonemura, S., Tsukita, S. and Tsukita, S. (1994). Perturbation of cell adhesion and microvilli formation by antisense oligonucleotides to ERM family members. The Journal of Cell Biology 125, 1371-1384.

Figure 1

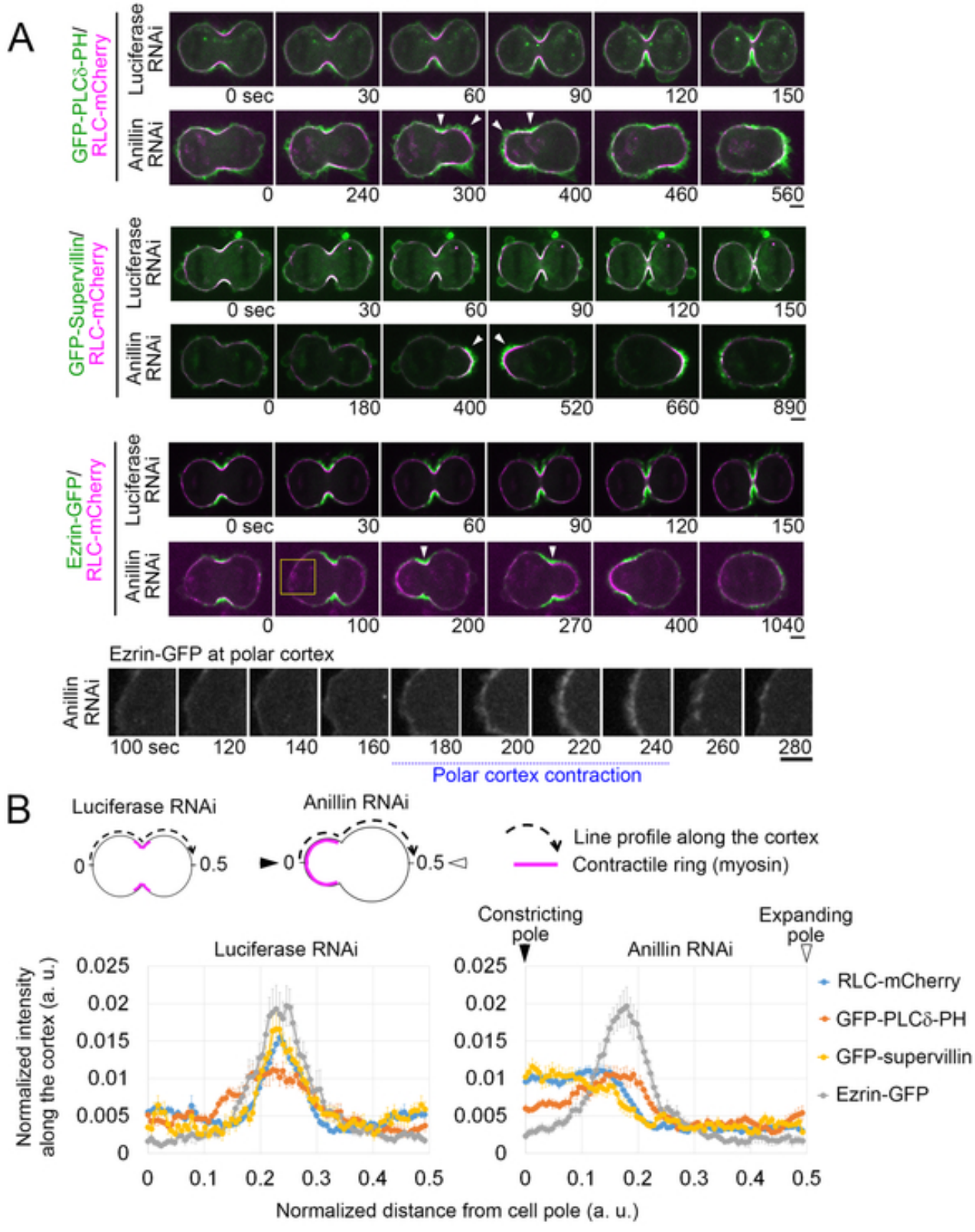
A
GFP-PLCδ-PH/ RLC-mCherry
Luciferase RNAi
0 sec 30 60 90 120 150
Anillin RNAi
0 240 300 400 460 560
GFP-Supervillin/ RLC-mCherry
Luciferase RNAi
0 sec 30 60 90 120 150
Anillin RNAi
0 180 400 520 660 890
Ezrin-GFP/ RLC-mCherry
Luciferase RNAi
0 sec 30 60 90 120 150
Anillin RNAi
0 100 200 270 400 1040
Ezrin-GFP at polar cortex
Anillin RNAi
100 sec 120 140 160 180 200 220 240 260 280
Polar cortex contraction
B
Luciferase RNAi
Anillin RNAi
0 0.5
Line profile along the cortex
Contractile ring (myosin)
Constricting pole
Expanding pole
Luciferase RNAi
Anillin RNAi
Normalized intensity along the cortex (a. u.)
0.025 0.02 0.015 0.01 0.005 0
0 0.1 0.2 0.3 0.4 0.5
Normalized distance from cell pole (a. u.)
RLC-mCherry
GFP-PLCδ-PH
GFP-supervillin
Ezrin-GFP

Figure 2

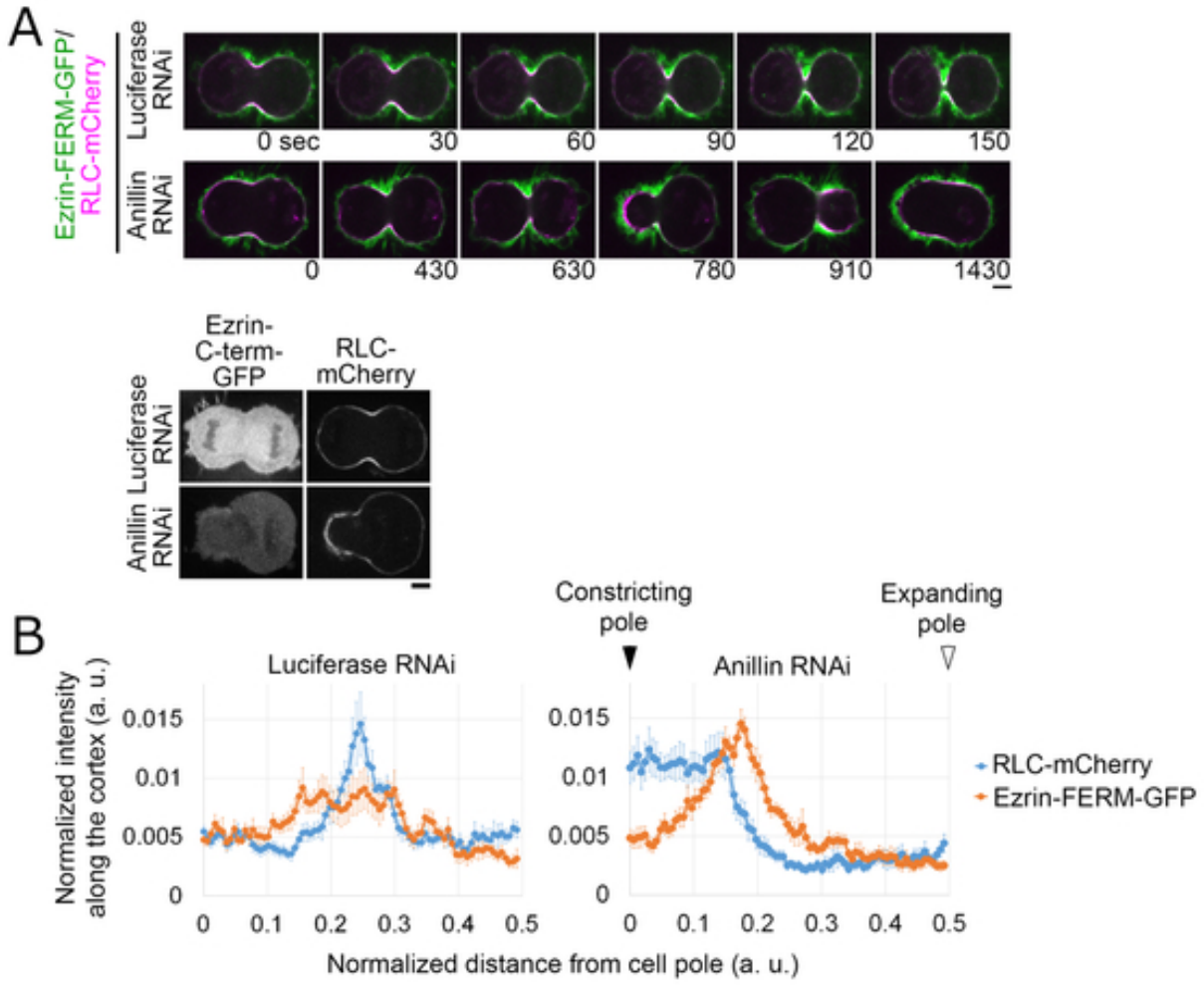
A
Ezrin-FERM-GFP/
RLC-mCherry
Luciferase RNAi
Anillin RNAi
0 sec
30
60
90
120
150
0
430
630
780
910
1430
Ezrin-C-term-GFP
RLC-mCherry
Luciferase RNAi
Anillin RNAi
B
Constricting pole
Expanding pole
Luciferase RNAi
Anillin RNAi
Normalized intensity along the cortex (a. u.)
0.015
0.01
0.005
0
0 0.1 0.2 0.3 0.4 0.5
RLC-mCherry
Ezrin-FERM-GFP
Normalized distance from cell pole (a. u.)

Figure 3

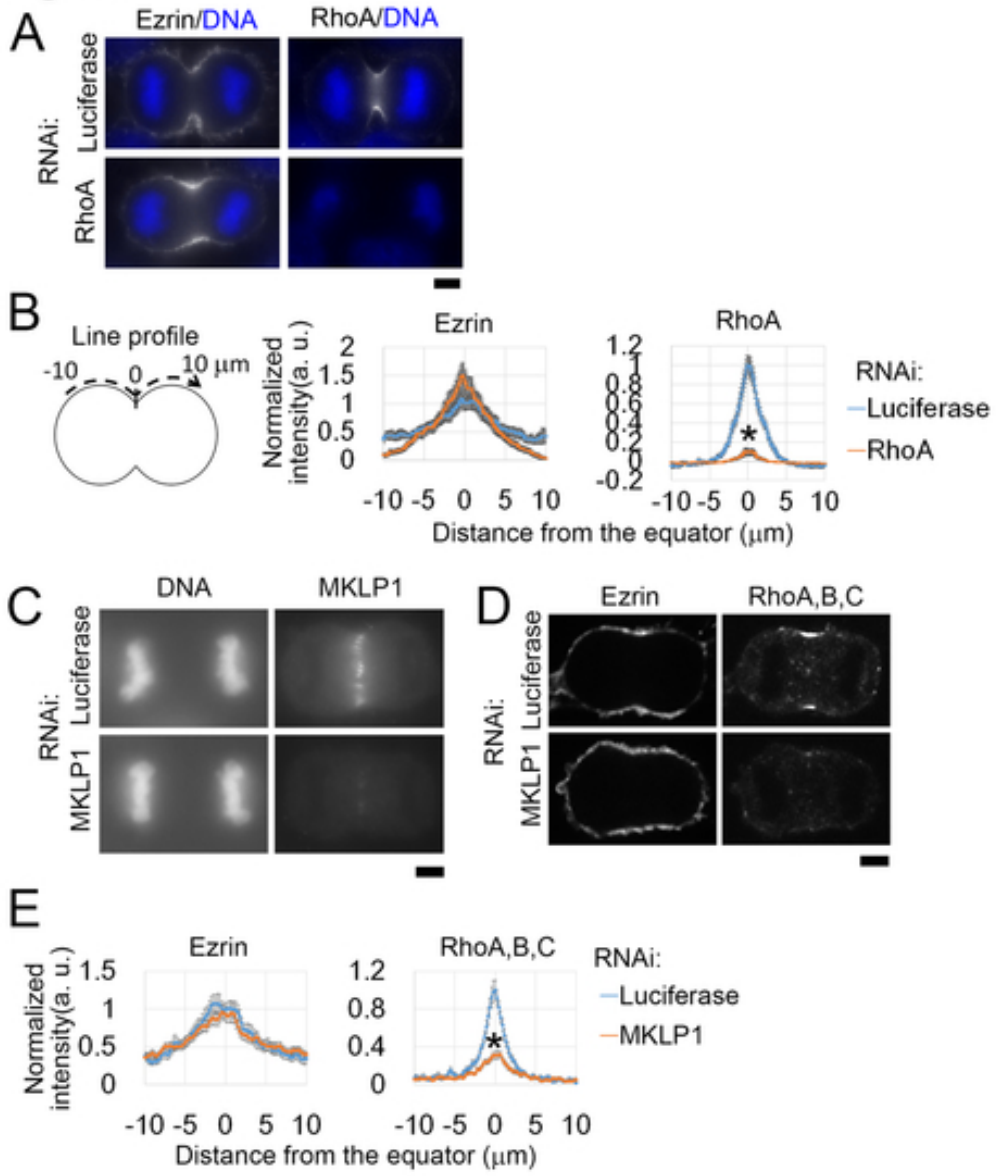
A
Ezrin/DNA
RhoA/DNA
RNAi:
Luciferase
RhoA
B
Line profile
-10
0
10 μm
Normalized intensity(a. u.)
Ezrin
RhoA
RNAi:
Luciferase
RhoA
Distance from the equator (μm)
C
DNA
MKLP1
RNAi:
Luciferase
MKLP1
D
Ezrin
RhoA,B,C
RNAi:
Luciferase
MKLP1
E
Ezrin
RhoA,B,C
Normalized intensity(a. u.)
RNAi:
Luciferase
MKLP1
Distance from the equator (μm)

Figure 4

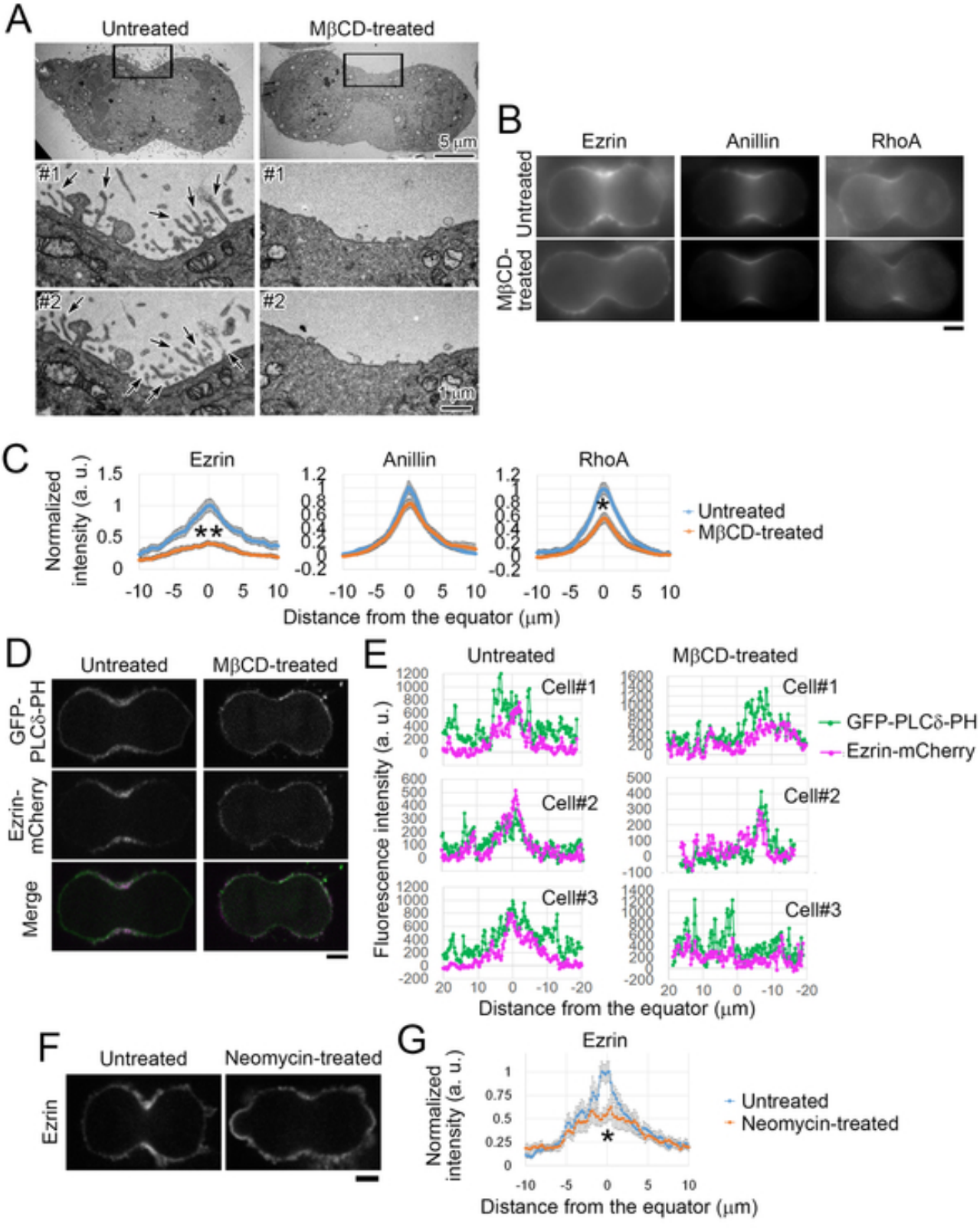
A
Untreated
MβCD-treated
5 μm
#1
#2
1 μm
B
Ezrin
Anillin
RhoA
Untreated
MβCD-treated
C
Ezrin
Anillin
RhoA
Normalized intensity (a. u.)
Untreated
MβCD-treated
Distance from the equator (μm)
D
Untreated
MβCD-treated
GFP-PLCδ-PH
Ezrin-mCherry
Merge
E
Untreated
MβCD-treated
Cell#1
Cell#2
Cell#3
Fluorescence intensity (a. u.)
GFP-PLCδ-PH
Ezrin-mCherry
Distance from the equator (μm)
F
Untreated
Neomycin-treated
Ezrin
G
Ezrin
Normalized intensity (a. u.)
Untreated
Neomycin-treated
Distance from the equator (μm)

Figure 5

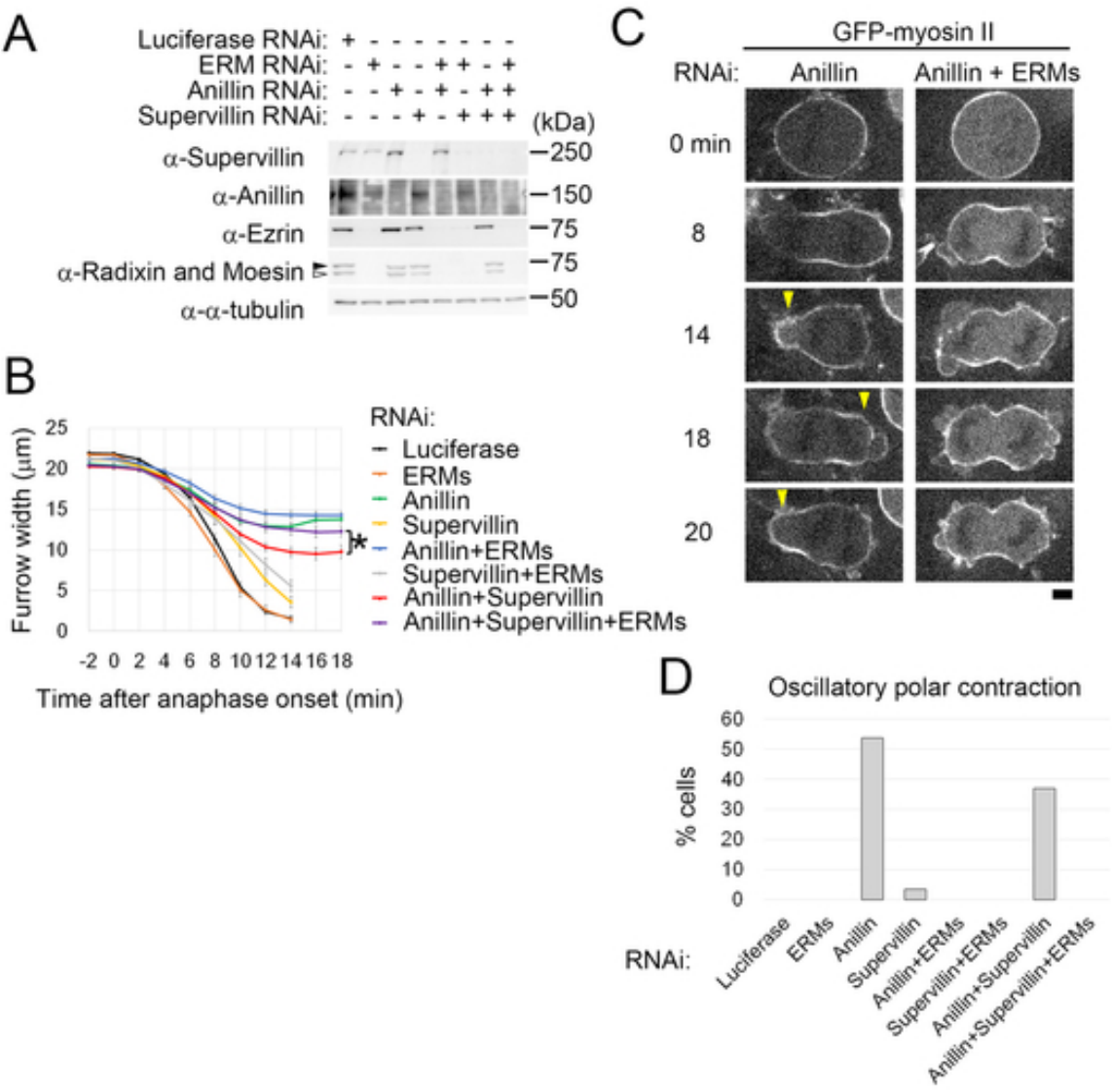
A
Luciferase RNAi: + - - - - - - -
ERM RNAi: - + - - + + - +
Anillin RNAi: - - + - + - + +
Supervillin RNAi: - - - + - + + +
(kDa)
α-Supervillin
α-Anillin
α-Ezrin
α-Radixin and Moesin
α-α-tubulin
250
150
75
75
50
B
Furrow width (μm)
25
20
15
10
5
0
-2 0 2 4 6 8 10 12 14 16 18
Time after anaphase onset (min)
RNAi:
Luciferase
ERMs
Anillin
Supervillin
Anillin+ERMs
Supervillin+ERMs
Anillin+Supervillin
Anillin+Supervillin+ERMs
C
GFP-myosin II
RNAi:
Anillin
Anillin + ERMs
0 min
8
14
18
20
D
Oscillatory polar contraction
% cells
60
50
40
30
20
10
0
RNAi:
Luciferase
ERMs
Anillin
Supervillin
Anillin+ERMs
Supervillin+ERMs
Anillin+Supervillin
Anillin+Supervillin+ERMs

Figure 6

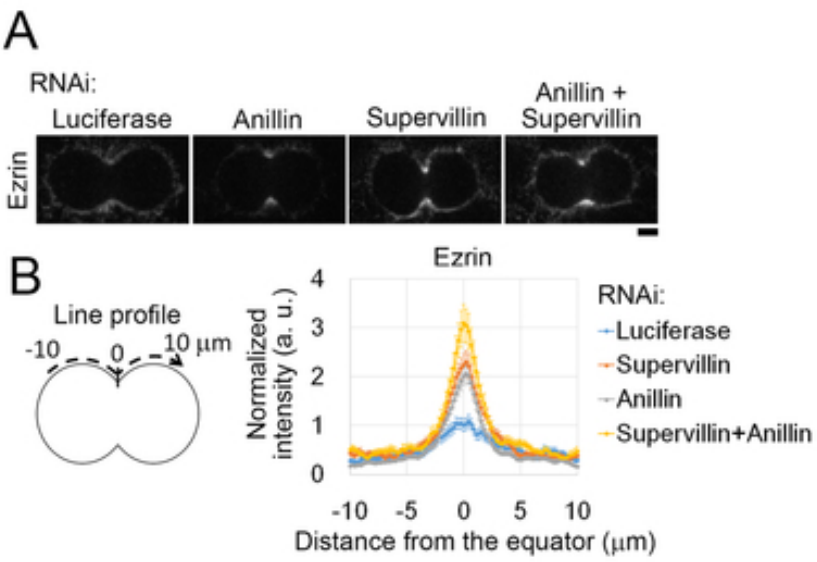
A
RNAi:
Luciferase
Anillin
Supervillin
Anillin +
Supervillin
Ezrin
B
Line profile
-10
0
10 µm
Ezrin
Normalized intensity (a. u.)
4
3
2
1
0
-10
-5
0
5
10
Distance from the equator (µm)
RNAi:
Luciferase
Supervillin
Anillin
Supervillin+Anillin

Figure S1

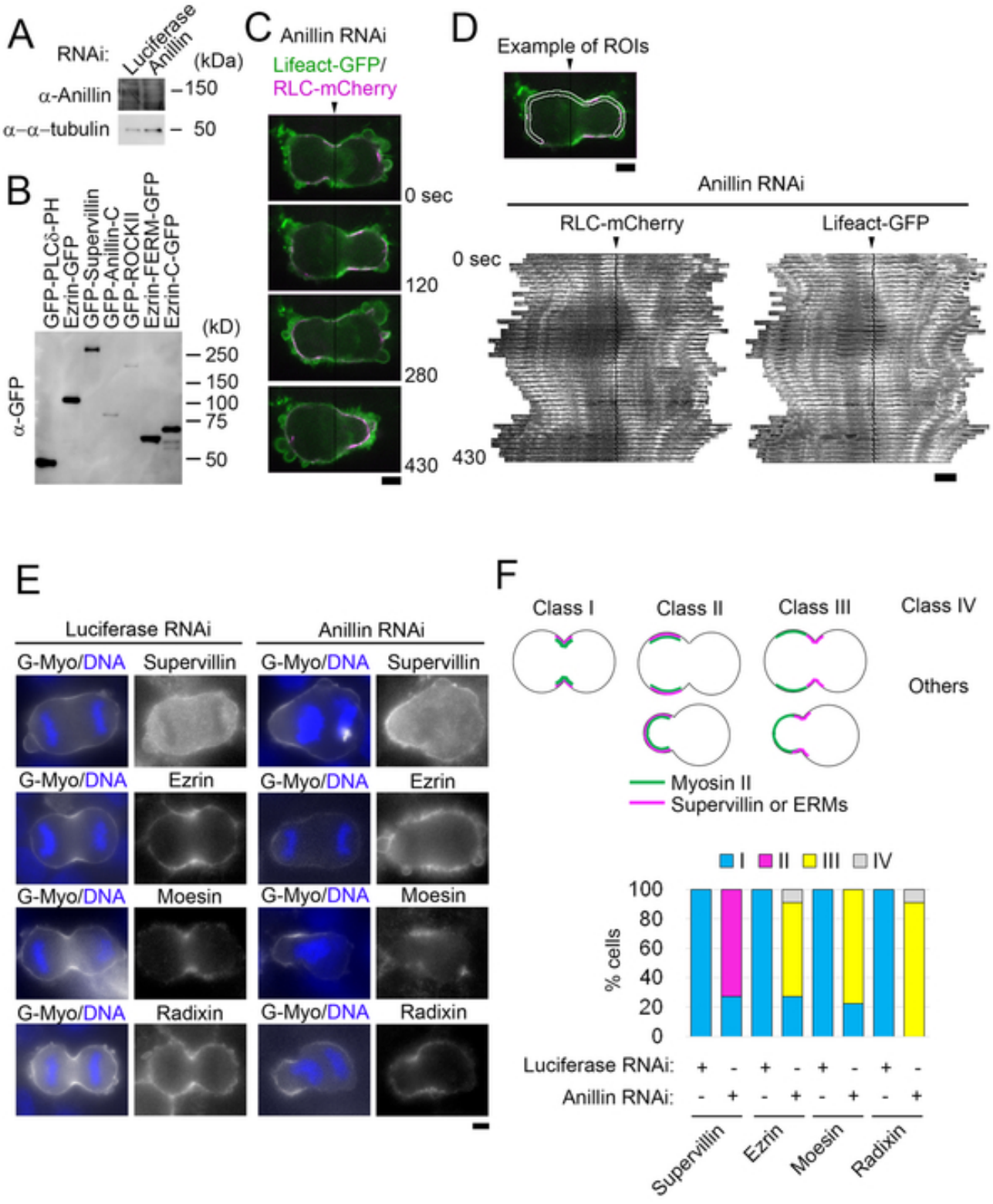
A
RNAi:
Luciferase
Anillin
(kDa)
α-Anillin
150
α–α–tubulin
50
B
GFP-PLCδ-PH
Ezrin-GFP
GFP-Supervillin
GFP-Anillin-C
GFP-ROCKII
Ezrin-FERM-GFP
Ezrin-C-GFP
(kD)
α-GFP
250
150
100
75
50
C
Anillin RNAi
Lifeact-GFP/
RLC-mCherry
0 sec
120
280
430
D
Example of ROIs
Anillin RNAi
RLC-mCherry
Lifeact-GFP
0 sec
430
E
Luciferase RNAi
Anillin RNAi
G-Myo/DNA
Supervillin
Ezrin
Moesin
Radixin
F
Class I
Class II
Class III
Class IV
Others
Myosin II
Supervillin or ERMs
I
II
III
IV
% cells
100
80
60
40
20
0
Luciferase RNAi:
Anillin RNAi:
Supervillin
Ezrin
Moesin
Radixin

Figure S2

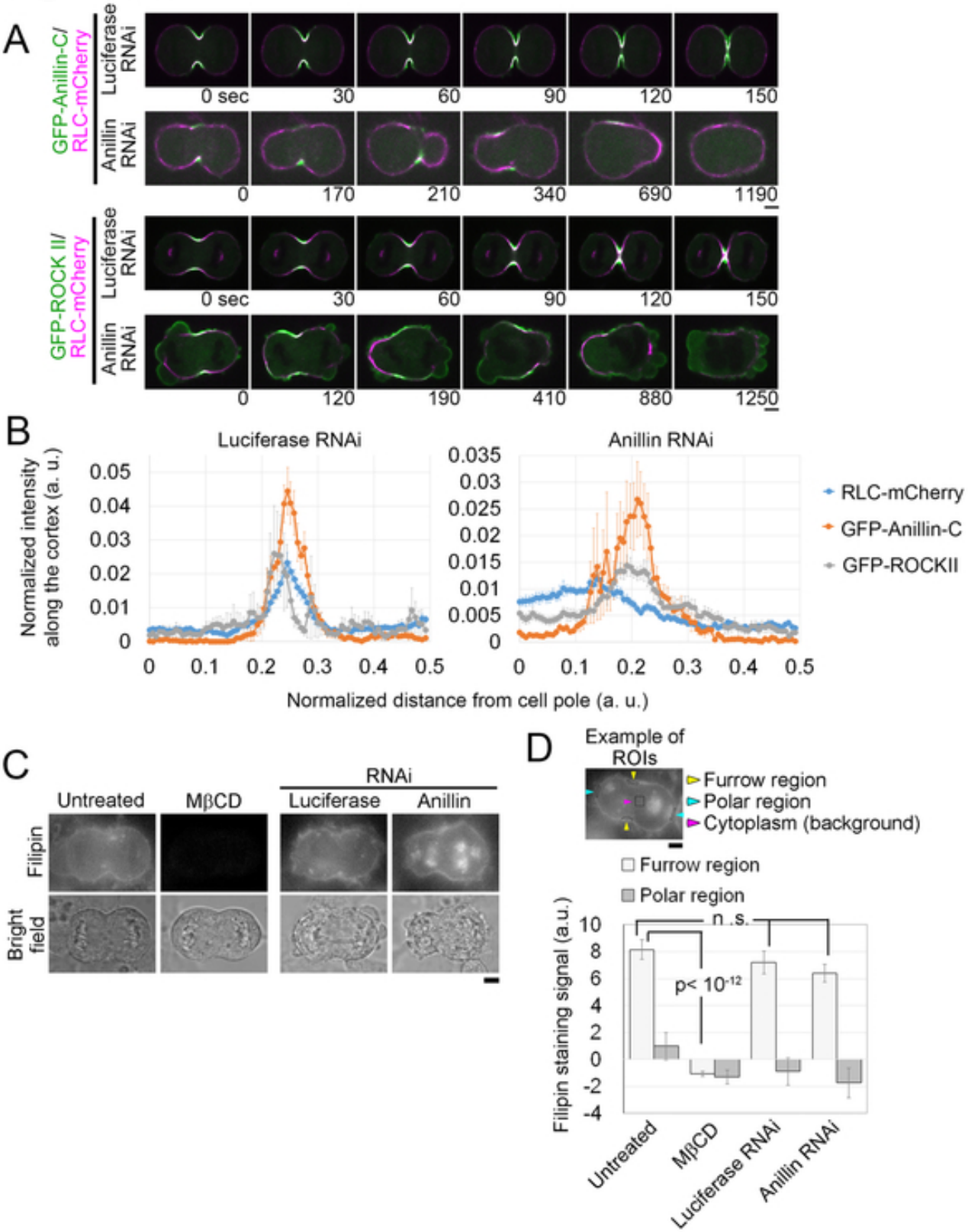
A
GFP-Anillin-C/ RLC-mCherry
Luciferase RNAi
Anillin RNAi
0 sec
30
60
90
120
150
0
170
210
340
690
1190
GFP-ROCK II/ RLC-mCherry
Luciferase RNAi
Anillin RNAi
0 sec
30
60
90
120
150
0
120
190
410
880
1250
B
Luciferase RNAi
Anillin RNAi
Normalized intensity along the cortex (a. u.)
Normalized distance from cell pole (a. u.)
RLC-mCherry
GFP-Anillin-C
GFP-ROCKII
C
RNAi
Untreated
MβCD
Luciferase
Anillin
Filipin
Bright field
D
Example of ROIs
Furrow region
Polar region
Cytoplasm (background)
Furrow region
Polar region
Filipin staining signal (a.u.)
n. s.
p< 10-12
Untreated
MβCD
Luciferase RNAi
Anillin RNAi

Figure S3

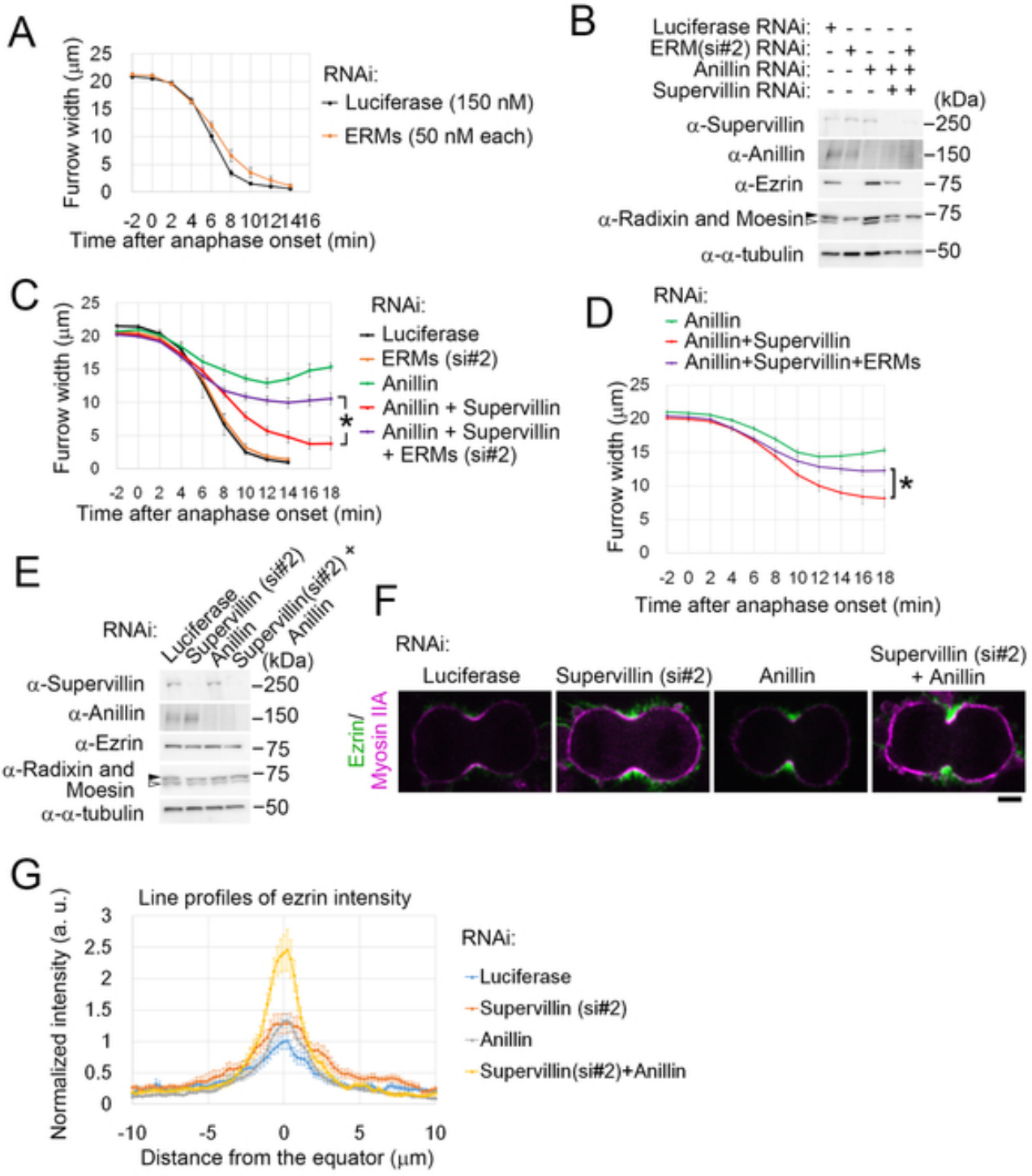
A
Furrow width (μm)
Time after anaphase onset (min)
RNAi:
Luciferase (150 nM)
ERMs (50 nM each)
B
Luciferase RNAi:
ERM(si#2) RNAi:
Anillin RNAi:
Supervillin RNAi:
(kDa)
α-Supervillin
α-Anillin
α-Ezrin
α-Radixin and Moesin
α-α-tubulin
C
Furrow width (μm)
Time after anaphase onset (min)
RNAi:
Luciferase
ERMs (si#2)
Anillin
Anillin + Supervillin
Anillin + Supervillin + ERMs (si#2)
D
RNAi:
Anillin
Anillin+Supervillin
Anillin+Supervillin+ERMs
Furrow width (μm)
Time after anaphase onset (min)
E
RNAi:
Luciferase
Supervillin (si#2)
Anillin
Supervillin(si#2)+Anillin
(kDa)
α-Supervillin
α-Anillin
α-Ezrin
α-Radixin and Moesin
α-α-tubulin
F
RNAi:
Luciferase
Supervillin (si#2)
Anillin
Supervillin (si#2) + Anillin
Ezrin/ Myosin IIA
G
Line profiles of ezrin intensity
Normalized intensity (a. u.)
Distance from the equator (μm)
RNAi:
Luciferase
Supervillin (si#2)
Anillin
Supervillin(si#2)+Anillin

Table S1: A list of siRNA used in this study

Target gene	Sequence (sense strand) (DNA hangover is in lower case)	References
Anillin	CGAUGCCUCUUUGAAUAAAtt	[1]
Supervillin (si#1)	GAGAACAAGGGAAUGUUGAGAGAat	
Supervillin (si#2)	GAAUCAACCUUUCUACCUUAAUAtc	
Ezrin (si#1)	CGUGGGAUGCUCAAAGAUAtt	
Ezrin (si#2)	GGAAUCAACUAUUUCGAGAtt	[2]
Radixin (si#1)	GGAAGAACGUGUAACCGAAtt	
Radixin (si#2)	GAACUAUACAUGCGAAGAAtt	
Moesin (si#1)	GGCUGAAACUCAAUAAGAAtt	[3]
Moesin (si#2)	CAUGCCCAAAACGAUCAGUtt	
RhoA	GCCGGUGAAACCUGAAGAAtt	[4]
MKLP1	AAGCAGUCUUCCAGGUCAUCUUU	[5]
Luciferase	CGUACGCGGAAUACUUCGAtt	[6]

References:

[1] Piekny, A.J. and Glotzer, M. (2008). Anillin is a scaffold protein that links RhoA, actin, and myosin during cytokinesis. Curr Biol 18, 30-6.

[2] Kvalvaag, A.S., Pust, S., Sundet, K.I., Engedal, N., Simm, R. and Sandvig, K. (2013). The ERM Proteins Ezrin and Moesin Regulate Retrograde Shiga Toxin Transport. Traffic 14, 839-852.

[3] Chirivino, D., Del Maestro, L., Formstecher, E., Hupé, P., Raposo, G., Louvard, D. and Arpin, M. (2011). The ERM proteins interact with the HOPS complex to regulate the maturation of endosomes. Molecular Biology of the Cell 22, 375-385.

[4] Yüce, Ö., Piekny, A. and Glotzer, M. (2005). An ECT2–centralspindlin complex regulates the localization and function of RhoA. The Journal of Cell Biology 170, 571-582.

[5] Douglas, M.E., Davies, T., Joseph, N. and Mishima, M. (2010). Aurora B and 14-3-3 coordinately regulate clustering of centralspindlin during cytokinesis. Curr Biol 20, 927-33.

[6] Uehara, R., Kamasaki, T., Hiruma, S., Poser, I., Yoda, K., Yajima, J., Gerlich, D.W. and Goshima, G. (2016). Augmin shapes the anaphase spindle for efficient cytokinetic furrow ingression and abscission. Mol Biol Cell 27, 812-27.

Table S2: A list of plasmid constructed in this study

Plasmid name	Insert (GenBank accession no.)	Vector	Cloning sites	Primers
pEGFP-ezrin/ pmCherry-ezrin	Ezrin, full length (NM_001111077.1)	pEGFP-N1/ pmCherry-N1	HindIII/ SalI	5′-ATAAAGCTTCACCATGCCGAAACCAATCAATGTCCGAG-3′ 5′-ATAGTCGACTGCAGGGCCTCGAACTCGTCGATGC-3′
pEGFP-ezrin-FERM	Ezrin truncate (NM_001111077.1) 1-309 a.a.	pEGFP-N1	HindIII/ SalI	5′- ATAAAGCTTCACCATGCCGAAACCAATCAATGTCCGAG -3′ 5′- ATAGTCGACTGGGCCTGGGCCTTCATCTGCTGCACC -3′
pEGFP-ezrin-C-terminal	Ezrin truncate (NM_001111077.1)296-586 a.a.	pEGFP-N1	HindIII/ SalI	5′- ATAAAGCTTCACCATGAAGCCTGACACCATCGAGGTGC -3′ 5′- ATAGTCGACTGCAGGGCCTCGAACTCGTCGATGC -3′
pEGFP-Supervillin	Supervillin, full length (NM_003174.3)	pEGFP-C1	SacI/ SacII	5′-ATAGAGCTCAAATGAAAAGAAAAGAAAGAATTGCCAGGCGCC-3′ 5′-ATACCGCGGTCAGAACAGGCCTTTTGCTTTCTTCAGGTTCACC -3′
pEGFP-Anillin-Cterminal	Anillin truncate (NM_001284301.2) 571-1087 a.a.	pEGFP-C1	SacI/ SacII	5′-ATAGAGCTCAAATGTTACTTGCACCATTGGCACAAACAG -3′ 5′- ATACCGCGGTTAAGGCTTTCCAATAGGTTTGTAGCAAGC -3′
pmCherry-RLC	MYL12B, Full length (NM_001144944.1)	A custom-made vector with a gateway cassette and a C-terminus mCherry tag	Gateway LR cloning	5′-CACCATGTCGAGCAAAAAGGCAAAGACCAAGACCACC -3′ 5′-GTCATCTTTGTCTTTGGCTCCATGTTTCAGGATG -3′